ARTICLE IN PRESS

Available online at www.sciencedirect.com

ScienceDirect

ELSEVIER

Atmospheric Environment ▮ (▮▮▮▮) ▮▮▮–▮▮▮

ATMOSPHERIC ENVIRONMENT

www.elsevier.com/locate/atmosenv

A study of boundary layer behavior associated with high NO concentrations at the South Pole using a minisodar, tethered balloon, and sonic anemometer

W. Neff[a,*], D. Helmig[b], A. Grachev[c], D. Davis[d]

[a]*NOAA Earth System Research Laboratory, 325 Broadway, Boulder, CO 80305, USA*

[b]*Institute of Arctic and Alpine Research, University of Colorado at Boulder, UCB 450, Boulder, CO 80309, USA*

[c]*Cooperative Institute for Research in Environmental Sciences, University of Colorado and NOAA Earth System Research Laboratory, 325 Broadway, Boulder, CO 80305, USA*

[d]*Georgia Institute of Technology, Atlanta, GA 30332, USA*

Received 30 June 2006; received in revised form 19 January 2007; accepted 20 January 2007

Abstract

This paper focuses on the use of an acoustic sounder, or sodar, during the 2003 Antarctic Tropospheric Chemistry Investigation (ANTCI), to document the behavior of very shallow (<50 m) stable boundary layers thought to be one of the critical factors for explaining the very high levels of nitric oxide (NO) found in past field experiments at the South Pole. The use of a tethered balloon, profiling wind, temperature, NO, and ozone provided for a detailed interpretation of sodar data for the period 12–30 December 2003. For the same period, sonic anemometer 2-m turbulence measurements, averaged to 0.5 h, linked surface processes to the evolution of the boundary layer in response to changing radiative balance and synoptic weather changes. A mixing-layer detection method was developed and applied to half-hour average sodar amplitude profiles for the period 23 November–30 December 2003. These data also allowed for testing of simple diagnostic equations for the mixing-layer depth as well as estimates of vertical diffusion rates under stable conditions, the latter being important for the effective depth of the mixing layer vis-à-vis the nonlinear NO chemistry postulated from earlier analyses. With the extended sampling period, two sub-seasonal regimes were examined: (1) a late-December period, with the full suite of supporting measurements, where the earlier results that shallow mixing layers associated with light winds and strong surface stability can be among the dominant factors leading to high NO levels were repeated and (2) a late November period that revealed additional complexities with very high NO concentrations appearing at times in concert with higher winds, weaker surface stability, and deeper mixing layers. The latter results are only consistent with a more complicated picture of how NO can build to very high levels that involves invoking the previously expressed dependence of elevated NO levels on nonlinear NO_x ($NO_x = NO + NO_2$) chemistry, greater fluxes of NO_x from the snowpack than previously observed at the South Pole, and the potential for enhanced NO_x accumulation effects involving air parcels draining off the high plateau. The results of ANTCI from 2003 thus argue for more complete future observations of boundary layer conditions over the high Antarctic Plateau and determination of the spatial and temporal variability of

*Corresponding author. Tel.: +1 303 497 6265; fax: +1 303 497 6020.
E-mail address: william.neff@noaa.gov (W. Neff).

1352-2310/$ - see front matter
doi:10.1016/j.atmosenv.2007.01.033

snow nitrate concentrations over the high plateau and their relation to NO recycling and the snow accumulation/ablation/erosion cycle.

Keywords: South Pole; Polar chemistry and meteorology; Sodar; Boundary-layer height

1. Introduction

Observations in the Austral Spring of 1998 during the Investigation of Sulfur Chemistry in the Antarctic Troposphere (ISCAT) project at the South Pole revealed unexpectedly high near-surface concentrations of nitric oxide, [NO], linked to photodenitrification of the snow and subsequent flux of NO into the boundary layer (BL) (Davis et al., 2001). A follow-on study in the spring of 2000 stimulated further analysis that suggested that the extremely high [NO] could be explained by a combination of factors including non-linear chemical processes, shallow BLs, and NO_x accumulation in air parcels as they drain off the high plateau toward the South Pole (Davis et al., 2004). During the 2000 field program, surface turbulence data were collected using a sonic anemometer. These were then used to estimate the boundary layer heights over nearly a two-week period using empirical relations based on similarity theory and analyses of spectral and cospectral behavior (Oncley et al., 2004). Comparison of [NO] with inferred depths revealed an inverse relationship (Davis et al., 2004). However, the inferred depths of ~50 m at high [NO] of ~500 pptv were not altogether consistent with the predictions of Davis et al. (2004) who suggested that such high concentrations would be more in-line with depths of ~20 m, based on a fixed NO_x flux estimate of 3.9×10^8 molecules $cm^{-2}\,s^{-1}$ (Oncley et al., 2004). To address the need to provide independent confirmation of the BL depth, several profiling techniques were used during a more recent field program carried out in the austral summer of 2003, the Antarctic Tropospheric Chemistry Investigation (ANTCI: Eisele et al., 2007). To provide continuous measurements of the BL, a high-resolution, short-range (15-180 m) acoustic sounder (minisodar) was deployed for the full experimental period. Routine wind (1 level) and temperature (3 levels) were measured on the station's 22-m tower. Twice-daily rawinsondes were also available. For the last two and a half weeks of the program, tethered-balloon measurements provided a series of temperature and wind profiles together with profiles of ozone (O_3) and NO along with sonic anemometers providing surface fluxes of sensible heat and momentum (Helmig et al., 2007a). We describe here the results from the analysis of these measurements and the insight they provide into the behavior of the BL at the South Pole and its effect on surface [NO].

2. Boundary layer measurement methods

The ANTCI experiment was carried out at the South Pole in the Atmospheric Research Observatory (ARO) building, and as shown in Fig. 1, both the meteorological tower and sodar systems were about 100 m from this building. In general, the South Pole is characterized by very persistent surface winds from the northeast throughout the year due to a combination of katabatic forcing

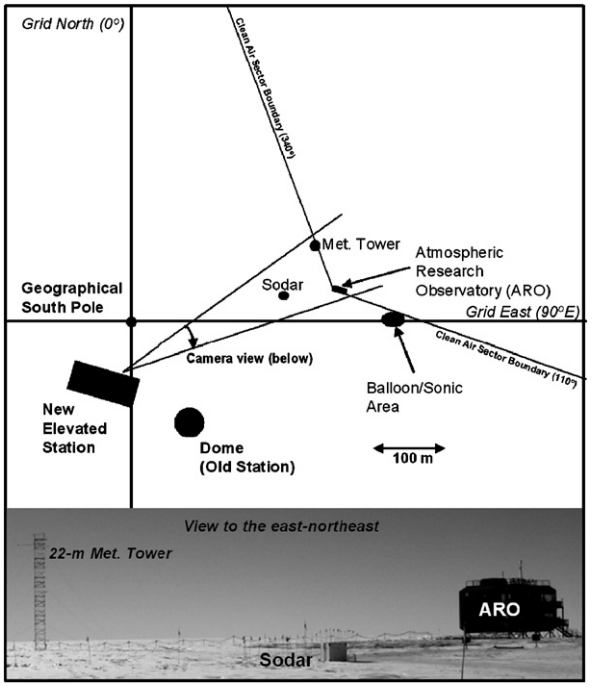

Fig. 1. Map of facility and instrument locations together with view from the new station to the east–northeast showing the 22-m meteorological tower, sodar, and Atmospheric Research Observatory (ARO) building. Photo courtesy of D. Gottas, NOAA/ESRL.

Please cite this article as: Neff, W., et al., A study of boundary layer behavior associated with high NO concentrations at the South Pole using a minisodar, tethered balloon, and..., Atmospheric Environment (2007), doi:10.1016/j.atmosenv.2007.01.033

(arising from the presence of a temperature inversion overlying a sloped surface) and the typically downslope orientation of the synoptic-scale pressure gradient at the South Pole (Neff, 1980). This persistence has been exploited to avoid contamination of air samples for atmospheric monitoring by designating the area from 340° to 110° as a "clean air sector." Measurements were thus located on the boundaries of this sector as shown in the figure. The suite of instruments and analysis methods described below were designed to monitor the state of the BL to aid in the interpretation of processes that may lead to high [NO]. For the purposes of this paper we will take the BL to be the turbulent layer nearest the surface that provides fluxes of momentum and heat to/from the surface. It should be noted that although there may be a shallow temperature inversion associated with this surface-based BL, it is often a component of a deeper inversion layer that results from large-scale weather processes (Neff, 1980).

2.1. Minisodar

Acoustic sounders, or sodars for sound detection and ranging, operate by transmitting a short burst of sound in a focused direction in the atmosphere and then listening for a signal scattered back from turbulence-induced acoustic refractive index structure. Sodars that operate at higher frequencies, short ranges, short transmitted pulses, and/or with smaller antennas are often referred to as "minisodars." A minisodar was deployed at the South Pole from November 18 to December 27, 2003. It was located about 140 m west of the ARO. The sound source was a compression driver located at the focal point of a parabolic dish some 1.2 m in diameter. A separate receiving antenna system was located next to the transmitting antenna: this so-called bistatic arrangement reduced the effect of reverberations in the system and provided a lower minimum range. When the antennas were first deployed on the snow surface we found a minimum range of about 4 m. However, when the antennas were elevated to avoid drifting of snow, the minimum range increased to about 14 m because of reverberation of sound between the antenna and the snow surface.

The operating frequency was 2100 Hz, the pulse repetition period was 1.18 s, and the pulse length was 0.020 s. The pulse length of 0.020 s provided a resolution of about 3 m whereas the period of the sounding gave a maximum range of about 180 ± 2.5 m, depending on air temperature. In the course of one hour approximately 3000 scans are accumulated to provide a detailed time-height cross-section of the strength of the scattered signal. The latter documents in great detail the behavior of the BL.

The backscattering itself arises from the interaction of the acoustic wave with small scale (one-half the wavelength of the sound, which is usually a few tens of centimeters) turbulent refractive index variations (mostly temperature). In idealized, statically stable conditions the scattering can be approximated by the equation (Neff, 1988):

$$\sigma = 0.01649 \frac{k_\lambda^{1/3}}{T^2} K_H^{2/3} \left(\frac{Rf}{1-Rf}\right)^{1/3} \left(\frac{\partial\theta}{\partial z}\right)^{5/3}, \quad (1)$$

where σ is the scattering cross-section per unit volume per unit solid angle, k_λ the acoustic wave number for wavelength λ, K_H the eddy diffusion coefficient for temperature given by the relation $\overline{w'\theta'} = -K_H \partial\theta/\partial z$, where the covariance of vertical velocity and potential temperature fluctuations is the vertical potential temperature flux, T the absolute temperature, Rf the flux Richardson number, and θ the potential temperature. The flux Richardson number is given by

$$Rf = Ri\left(\frac{K_H}{K_M}\right), \quad (2)$$

where K_M is given by $\overline{u'w'} = -K_M \partial U/\partial z$ (u' is the fluctuation in the horizontal wind speed, aligned along the mean wind direction, and w' the fluctuation in vertical velocity; U is aligned along the mean wind direction) and the gradient Richardson number Ri for a dry atmosphere is given by

$$Ri = \frac{g}{T} \frac{\partial\theta/\partial z}{\left[(\partial U/\partial z)^2 + (\partial V/\partial z)^2\right]}, \quad (3)$$

where g is 9.8 m s^{-2}, T is the absolute temperature, U and V are the horizontal components of the mean wind, and $\partial\theta/\partial z$ is the potential temperature gradient, which is the normal temperature gradient plus an adiabatic correction of about +0.98 °C/100 m. From Eqs. (1)–(3), several aspects of the acoustic scattering under statically stable conditions can be seen:

- Noting the weak dependence on the term in Eq. (1) involving Rf, the strongest sensitivity is to the vertical potential temperature profile but turbulence must exist ($K_H > 0$) to produce a

Please cite this article as: Neff, W., et al., A study of boundary layer behavior associated with high NO concentrations at the South Pole using a minisodar, tethered balloon, and..., Atmospheric Environment (2007), doi:10.1016/j.atmosenv.2007.01.033

return signal from any given region of the atmosphere. In a statically stable atmosphere, spatially and temporally intermittent turbulence will produce isolated regions of scattering. Near the surface there should also be a region of turbulence produced by wind shear that results from surface friction. We will take the top of this layer as the top of the boundary layer.

- K_H should also be sensitive to the vertical potential temperature profile, i.e. increasing stability should reduce the eddy diffusion for the same wind shear. Thus, Eq. (1) indicates a fairly nonlinear response to the vertical temperature gradient.
- At small *Ri* (due to strong wind shear or weak potential temperature gradients) the scattering is small; similarly, at larger *Ri*, the scattering should be reduced because of decreasing K_H. Application of a second-order turbulence closure model confirms this behavior as shown by (Neff, 1988).

In contrast to the stable case, the so-called "free-convection" case predicts that the acoustic scattering will falloff with height z as $Q_o^{4/3}z^{-4/3}$where Q_o is the surface heat flux (Wyngaard et al., 1971). Although rare, there are periods at the South Pole where convection does occur, sometimes during cold frontal passages when the air is relatively colder than the underlying snow surface or in the presence of warm clouds aloft that shift the radiative balance toward a net heat input to the snow. In addition, in these cases, the overlying atmosphere is usually statically stable and the convection erodes into this statically stable layer, creating a capping inversion layer. The fact that Q_o is typically quite small under South Pole conditions allows convective BL echo-profiles to be discriminated from stable BL echo-profiles by virtue of small signal strength.

2.2. Tethered balloon

The tethered balloon operations during the experimental period have been described in detail by Helmig et al. (2007a). In summary, the balloon site was located about 100 m southeast of the ARO with 128 profiles (ascent and descent) obtained from 10 December to 31 December. Both O_3 and NO were measured from the balloon. Temperature, wind speed and direction, relative humidity, and pressure were measured using a Vaisala TSP-5A-SP tethersonde, which transmits to a ground station. The ascent rate was typically 0.2–0.3 m s^{-1}, with a typical 1–2 s response time for the balloon temperature and wind sensors. Typically, two to four samples were collected over each meter of height and then averaged over two and five meters. The O_3 sensor had a response of about 30 s which was clearly evident in comparing ascent and descent profiles. The NO measurements were corrected for long-sampling-line delays as described by Helmig et al. (2007b). The balloon was raised and lowered using a winch which was heated to maintain its hydraulic fluids at an appropriate operating temperature. Under very light wind conditions (<2 m s^{-1}) temperatures during ascent were observed to be high by about 1 °C for the first 10–20 m, possibly because of the longer residence time of the sensor package in the vicinity of the winch prior to launch. For this reason, only descents were used to calculate stability as presented in our figures. Another source of error occurs under light wind conditions with significant azimuthal shear: in these situations, the balloon on descent can be drawn across the mean wind, adding a transverse wind component and an error in wind direction of on the order of 20°. However, the local variation with height appeared to be unaffected in the calculation of the local Richardson number. Supplementary wind and temperature sounding data were also available from the twice-daily rawinsonde launches at the station. These used a Vaisala GPS-based system which produces much lower resolution data than the tethered balloon package because of its faster ascent rate.

2.3. Surface meteorology

Routine meteorological data were collected from the 22-m tower located about 100 m to the north-northeast of the ARO. This facility is operated by the Global Monitoring Division (GMD) of the Earth System Research Laboratory at NOAA. Wind was recorded at 17 m while aspirated temperature data were collected at 2, 13, and 22 m. The temperature at 13 m was only recorded with 0.1 °C resolution and therefore is not used in subsequent gradient calculations. These data were nominally averaged to 1-h intervals although special ANTCI recording occurred at 10-min averaging intervals. In addition, simultaneous measurements from the ARO of NO were made at ~10 m and O_3 at 17 m above the snow surface for the same 10-min

Please cite this article as: Neff, W., et al., A study of boundary layer behavior associated with high NO concentrations at the South Pole using a minisodar, tethered balloon, and..., Atmospheric Environment (2007), doi:10.1016/j.atmosenv.2007.01.033

intervals for the entire experimental period. The GMD also collects radiation data including up- and down-welling infrared radiation, as well as solar downwelling and reflected radiation. These provided data with which to separate effects of radiative changes from advective ones on BL structure.

2.4. Turbulence

An additional 2-m tower was also set up near the tethered balloon sounding site with a conventional cup and vane anemometer, an aspirated thermocouple temperature sensor, and a 3-axis sonic anemometer (CSAT-3, Campbell Sci., Logan, UT) that was provided courtesy of the National Center for Atmospheric Research. The data were processed as described in more detail by Cohen et al. (2007). The sonic anemometer data were processed in one-half hour blocks to assure reasonably stable spectral estimates and to match the averaging time for mixing-layer heights determined from time-averaged sodar data. The data were quality controlled through inspection of the behavior of the spectra and cospectral. "Errors" in the sonic data are typically in the realm of electronic noise (spiking) or those associated with a limited time average. For wind directions ranging from east to southeast, the sonic was downwind of the tethered balloon winch, creating the potential for thermal contamination. Under light easterly wind conditions, upward heat fluxes were occasionally observed despite overall strong static stability as recorded on the 22-m tower several hundred meters distance away. These data were rejected for further use.

3. Mixing layer interpretation and diagnostics

3.1. Overview

The experimental period extended from mid-November through late December. Fig. 2 indicates, schematically, the daily average cloud cover, the vertical temperature differences from the 22 m tower, and the periods of operation of key instrument systems. Two periods of moderate-to-strong stability were selected for more detailed analyses. The early period during Days 325–339 (21 November–5 December) was characterized by partly-cloudy to clear conditions. The late period with nearly clear

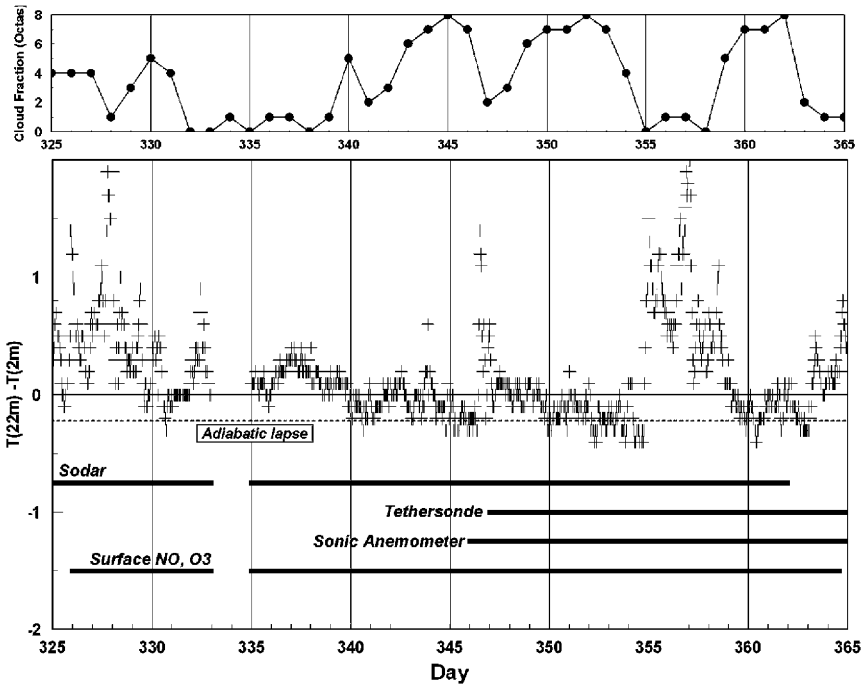

Fig. 2. Time series of daily cloud cover, temperature difference between 2 and 22 m, and operational periods for key measurement systems used in the current analysis. A general data gap occurred on Day 334. Two periods of strong stability (also coupled with light winds) occur; detailed analyses were possible in the second period, Day 355–359. Only a few periods are evident when convection is possible (T_{22}–$T_2 < -0.196$ °C: dashed line).

Please cite this article as: Neff, W., et al., A study of boundary layer behavior associated with high NO concentrations at the South Pole using a minisodar, tethered balloon, and..., Atmospheric Environment (2007), doi:10.1016/j.atmosenv.2007.01.033

conditions, Days 355–358 (21–24 December), followed a cloudy, windy, well-mixed regime that included periods of convective activity. This late period, with sonic anemometer and balloon profile information available, provided for detailed analyses of mixing layer behavior as described below.

3.2. Echo interpretation and processing

3.2.1. Low-level jet

Fig. 3 shows (a) typical profiles of wind speed, temperature, and [NO], (b) the Richardson number calculated with fine (2 m) and coarse (5 m) averaging, and (c) the corresponding sodar facsimile recording. The meteorological data were all obtained from a simultaneous tethersonde sounding that began its descent just before 0400 UTC as indicated in Fig. 3(c). The basic features of the surface mixing layer (to about 25 m with $Ri < 0.25$), a decrease in echo strength (just above 30 m, with $Ri > 1.0$), and sporadic turbulence above 40 m are evident. In many of such cases, the wind speed maximum is a region of large Richardson number, confining turbulence to the region below the jet. The jet phenomenon can be seen in the sodar record with Kelvin–Helmholtz billow-like echoes forming in the shear region below the jet. The slope of these structures indicates wind speed increasing with height, with the top of each billow appearing higher in the sodar beam first and then descending as the structures advect through the beam (Neff and Coulter, 1985). Conversely, with the wind decreasing with height above the jet, the slope of these structures is opposite. Above the primary echo layers, intermittent turbulent patches appear which indicate isolated regions of vertical mixing aloft. Because of the terrain slope at the South Pole, such low-level jets are a dominant feature of the boundary layer under clear-sky conditions.

Fig. 3 shows profiles of [NO] to 110 m, together with sodar and sounding data. In this case, high [NO] is confined to the lowest turbulent layer only

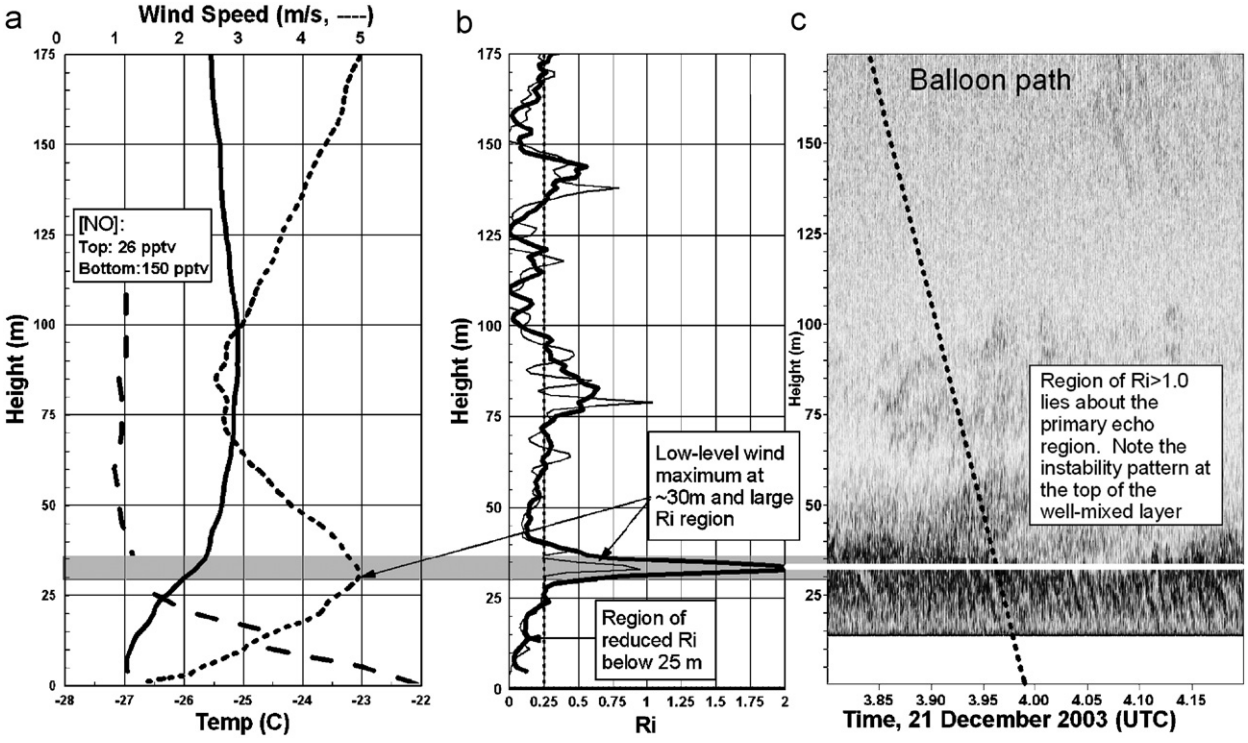

Fig. 3. December 21, 2003 (Day 355): (a) Tethersonde profile of smoothed wind speed (short dashed line), temperature (solid line), and profile of [NO] (long-dashed line). (b) Derived *Ri* with averaging over 2 m (thin line) and 5 m (thick line). $Ri = 0.25$ indicated by dashed line. Shading indicates where thermal stability is the greatest and where *Ri* is also large. (c) Sodar record showing this period in detail with the path of the tethered balloon approximated by the dashed line. Note that the primary sodar echoes appear below the height of maximum *Ri*. This fairly common event includes a low-level jet, instabilities (the herringbone pattern in the facsimile record) in the strong-shear region below the jet and a mixing layer near the surface.

Please cite this article as: Neff, W., et al., A study of boundary layer behavior associated with high NO concentrations at the South Pole using a minisodar, tethered balloon, and..., Atmospheric Environment (2007), doi:10.1016/j.atmosenv.2007.01.033

and the bulk amount of it is seen situated well below the height of the amplitude maximum from the sodar. In fact, the decrease of [NO] with height within the mixing layer is almost exponential in agreement with the numerical simulations of Wang et al. (2007). Thus, from the standpoint of determining the maximum height, through which NO might mix, this is one of the simplest situations.

3.2.2. Very stable surface layer

Fig. 2 revealed two periods with persistent strong surface stability, namely Days 325–330 and Days 355–358. Fig. 4 provides a more detailed look at one day under clear sky conditions (Day 356, 22 December 2003) during which stability increased and the mixing-layer depth decreased in the course of the day, coincident with a doubling of [NO] over about 12 h. Sodar facsimile records at the beginning, Fig. 4(a), and end of the day, Fig. 4(c), reveal how the mixing layer (marked by the surface-based echo layer) descends below the 22-m level on the meteorological tower during the day. This is consistent with an interpretation of the warming seen at 22-m, Fig. 4(b), as due to the descent of the inversion below that sensor level. Two periods of surface cooling at 2 m appear in Fig. 4(b): the cooling at midday coincides with a period of net radiation loss ($-10\,W\,m^{-2}$ with little change in wind

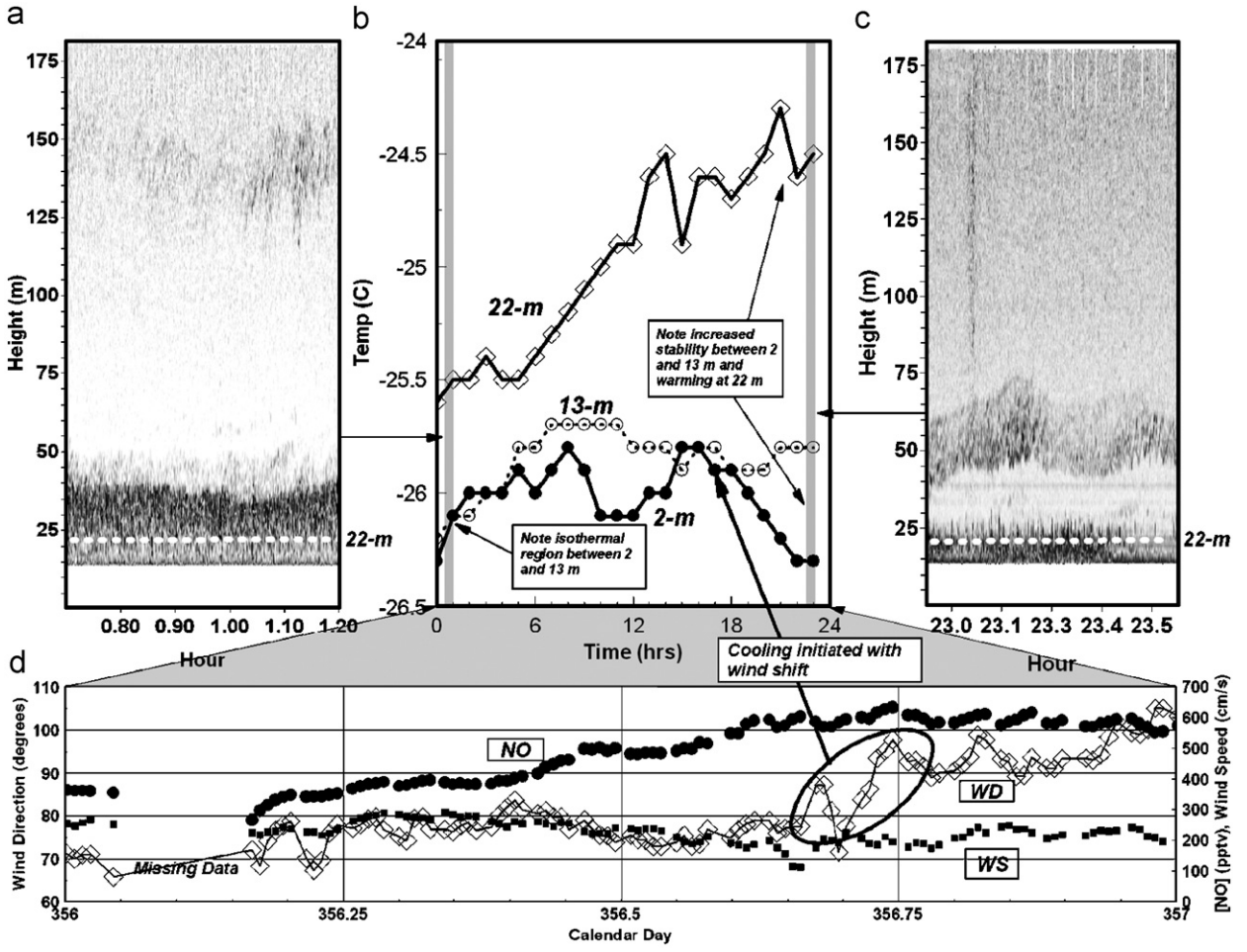

Fig. 4. Data from Day 356 (22 December 2003) showing the effect of increasing stability and decreasing mixing-layer depth on surface [NO]: (a) Sodar record from the beginning of the day showing a mixing layer extending well above the 22-m tower. (b) Time series of temperature at 2-, 13-, and 22-m through the day. Sodar sample intervals at the beginning and end of the day are indicated by vertical gray stripes. (c) Sodar record at the end of the day when the surface inversion and boundary layer have subsided below the 22-m level of the tower. (d) Time series of [NO], wind speed at 13 m (WS), and wind direction at 13 m (WD) showing a doubling of [NO] during a time when the wind speed remained relatively constant but the boundary layer depth decreased by about a factor of two. Note that the wind shift at 1600 UTC was associated with a decrease in temperature but not with any change in [NO].

Please cite this article as: Neff, W., et al., A study of boundary layer behavior associated with high NO concentrations at the South Pole using a minisodar, tethered balloon, and..., Atmospheric Environment (2007), doi:10.1016/j.atmosenv.2007.01.033

speed or direction) whereas the second occurs with a small positive radiation gain ($+5\,W\,m^{-2}$) as seen in GMD radiation data. During the latter period the wind direction (Fig. 4(d)) changes to a more downslope direction and presumably reflects an advective change in temperature. On 22 December, the daily climatology recorded clear sky conditions although hourly observer reports documented a few clouds present ⟨ftp://amrc.ssec.wisc.edu/pub/southpole/⟩. Micro-pulse lidar records also indicated clear sky conditions ⟨http://mplnet.gsfc.nasa.gov/⟩.

The wind profile during the day (not shown) evolved from a moderate ($5\,m\,s^{-1}$) jet at about 35 m to a profile with weak but multiple wind maxima at 15 and 40 m, corresponding to the two echo layers seen in Fig. 4(c). At higher levels, a well-defined jet was present above 100 m which then weakened and lifted above 150 m by the end of the day. During the same period, turbulence levels measured by the sonic anemometer decreased by a factor of two, with only a minor change in the 13-m wind speed. As we will show later, [NO] during this later period has a well-defined inverse relationship to surface stress.

3.2.3. Convection with a capping inversion

The vertical temperature difference in Fig. 2 showed that the surface layer during the ANTCI field experiment varied between very stable and convective conditions. In particular, on Day 353, there are a number of periods during which the temperature lapse rate is greater than the adiabatic rate, conductive to thermal convection from the surface and more efficient dilution of the surface fluxes of NO_x. On this day, cloud cover varied from solid overcast, to broken, to almost clear conditions. Inspection of net radiation data (not shown) reveal generally positive values that track the sensible heat flux in sign. Interestingly, upward sensible heat fluxes usually occur during cloud to partly cloudy conditions whereas, under clear sky conditions, radiative losses (in the infrared) from the surface exceed the gain from the incident solar radiation (Cohen et al., 2007; King et al., 2006) resulting in a surface temperature inversion.

Fig. 5 shows an analysis of sodar data for the period centered on 0400 UTC on Day 353. During this fairly rare convective event, the upward sensible heat flux accounts for about half of the net radiation available at the surface. The remaining radiative heat input should

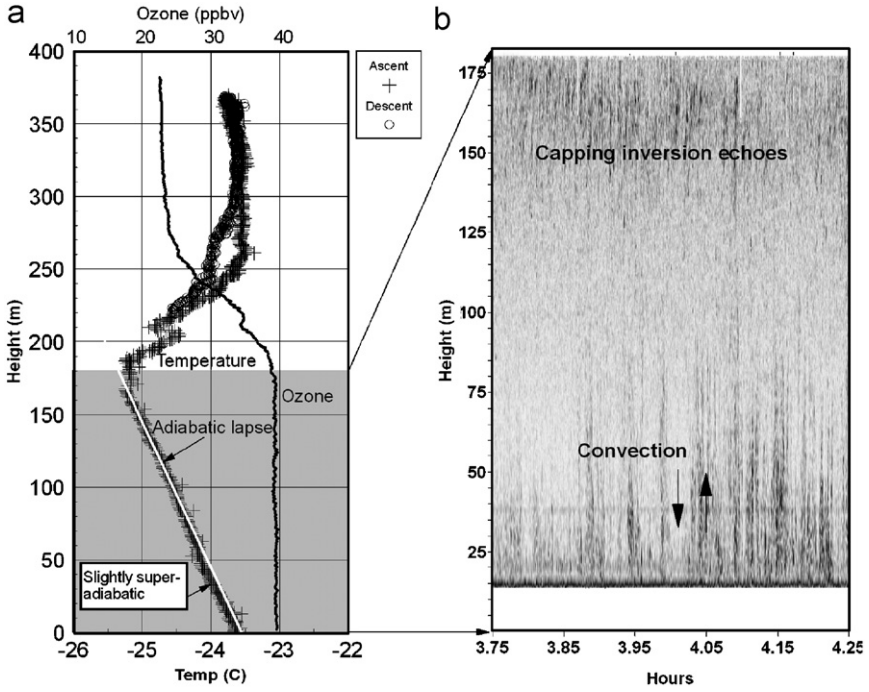

Fig. 5. (a) Convection with a capping inversion on Day 353 (19 December 2003) showing a nearly adiabatic lapse rate to 165 m with a capping inversion. (b) Corresponding sodar record (with a different height scale). The sodar height range is shown as shading in (a). The record shows convective plume echoes below 75 m and a layer of echoes above 150 m marking the beginning of the elevated temperature inversion.

Please cite this article as: Neff, W., et al., A study of boundary layer behavior associated with high NO concentrations at the South Pole using a minisodar, tethered balloon, and..., Atmospheric Environment (2007), doi:10.1016/j.atmosenv.2007.01.033

heat the snow in the short term. Normally, in the summer, the solar flux only serves to minimize radiative losses while the continuing sensible heat flux into the snow accounts for the major heat storage mechanism during summer (Carroll, 1982). In this case, the sodar record shows echoes characteristic of convective plumes while the temperature profile reveals an almost adiabatic layer that extends to about 165 m, just below a capping inversion. The isothermal layer appears to be the source of the echoes on the sodar record between 150 and 180 m. [NO] measurements (not shown) obtained during this event were made to a height of 85 m: concentrations were highest at the surface, ~73 pptv, and fell off to about 50 pptv at a height of 40 m. The ozone profile reveals that it is well mixed under the capping inversion with a falloff through the inversion. Because of the slow time constant for the O_3 sensors (~30 s: ~9 m at 0.3 m s^{-1}), the actual falloff would be somewhat faster than indicated.

3.3. Mixing-height estimation

The examples above reveal a broad range of BL states, from the simple to the complex, that are observed even in the ideal conditions at the South Pole (uniform fetch and no diurnal cycle). For purposes of explaining the BL mixing component to surface [NO] variations, we analyzed the sodar amplitude profile data averaged over 0.5 h so as to provide a comparison with surface turbulence measurements obtained over the same period. Fig. 6 summarizes the typical profiles that encompass most of the experimental period. In Fig. 6(a), three classes of deeper mixing-layer regimes are shown: (1) convective with no apparent capping inversion below the sodar's maximum range of 180 m, (2) convection with a capping inversion at or below 180 m, and (3) windy with weak-to-neutral stability. In each of these cases there is a "noise level" reference line. The reason for this reference level is that there is a range multiplier for the sodar amplitude to compensate for the spreading of the signal with range so as to create a realistic looking profile. Unfortunately, the sodar is also sensitive to the background noise, typically due to nearly constant wind effects on the antenna structure, which is then subject to the same ramp function. The noise level was determined by the total signal at the maximum range of the sodar; when

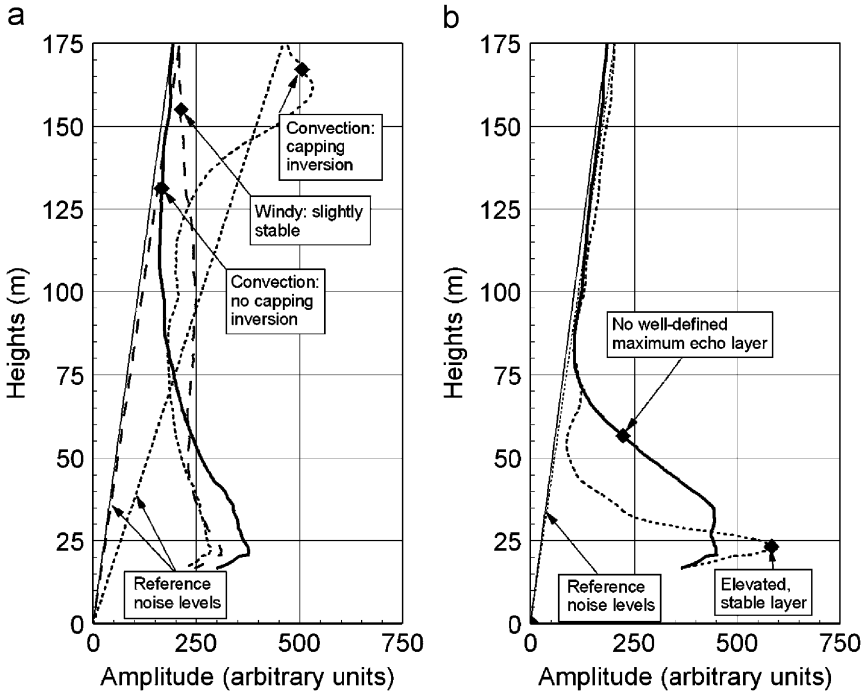

Fig. 6. Five basic echo profiles used to guide automated analysis of 0.5-h averaged sodar data. Mixing layer depths indicated by solid diamonds. (a) Convective (solid line), convective with a capping inversion (short-dashed line) and windy (long-dashed line) profiles: the depth was determined where the signal level approached within 15% of the background noise level (straight lines: coded the same as the echo profiles) working down from 175 m. (b) Stable cases: the height of the peak amplitude was used for the elevated echo layer (dashed line) whereas 50% of maximum amplitude was used when no well-defined maximum occurred (solid line).

Please cite this article as: Neff, W., et al., A study of boundary layer behavior associated with high NO concentrations at the South Pole using a minisodar, tethered balloon, and..., Atmospheric Environment (2007), doi:10.1016/j.atmosenv.2007.01.033

there are echoes present, these distort the reference profile as is the case with the situation of the "elevated" inversion in Fig. 6(a). In each of these cases the height was found, working from the top of the profile down, at which the signal level exceeded the background noise reference level by 15% (noted in the figure), a criterion that provided the most consistent results. In Fig. 6(b), two stable layer cases are shown. In these cases, the simplest approach, because of the echoes confined below 75 m, would be to pick the height at which the amplitude falls off to, say 50%, of its largest value. However in one of the profiles, a well-identified peak amplitude is present and then a falloff of echo amplitude above and below similar to that shown in Fig. 3, where the area of mixing (small Richardson number) was shown to be confined at heights below that of the peak. For this reason, the height of the peak was chosen as the mixing-layer height. In the second case, there is no distinct peak, so the height at which the amplitude fell to 50% of its maximum value was chosen as the mixing-layer height. The rationale for the 50% level was that the falloff of the average signal strength often represents movement of an echo layer with a distinct upper boundary up or down during the 0.5-h averaging period: the 50% level would thus represent the average height. In some very stable cases, with weak echoes, permanent echoes (due to reflections from nearby objects) can appear in the lowest 30 m of the sodar record and appear as a small perturbation of the profile and bias the peak-picking results: in these cases an amplitude-weighted height was used.

In the stable cases, the mixing-layer height determined from the sodar data can be viewed as an estimated upper boundary for mixing processes. Because acoustic scattering depends on both turbulence levels and the vertical temperature gradient, there is no direct comparison with the common "rule-of-thumb" for the stable boundary layer depth of a falloff of turbulence to 10% of its surface value. A final mixing height data set was generated following an examination of the time series for outliers using the raw profile averages as well as the original facsimile records.

4. Mixing-height/[NO] analyses

4.1. Sodar mixing height time series

Sodar estimates of the mixing-layer depth were available for the entire ANTCI 2003 experimental period as shown in Fig. 7(a). Altogether, there were 1873 0.5-h profiles generated. In 408 profiles, no mixing layer top was detected within the sodar range of 180 m. For the remaining 1437 profiles, the median mixing-layer depth was 59.0 m whereas the mean was 76.3 m with a standard deviation of 49.6 m. The lowest quartile was below 30.2 m.

Three periods of shallow BLs are evident, during Days 323–333, briefly on Day 346 (when chemical measurements at the ARO were contaminated by the station's power plant plume), and again on Days 355–359. These periods correspond to increased near-surface stratification as shown in Fig. 2 and as was observed in previous experiments (Davis et al., 2004). The time series of [NO] (Fig. 7(b)) and sodar mixing-layer depth for the experimental period (Fig. 7(a)) shows a generally inverse relationship similar to that found by Davis et al. (2004). However, for the period of Days 326–329, [NO] is somewhat higher for mixing-layer depths that are comparable to those seen at the end of December (Days 355–358). For Days 323–329, the average wind was $3.6\,m\,s^{-1}$ from 89° while the average temperature difference from 2 to 22 m was 0.47 °C. For the 8-day period prior to this episode, the average wind was $4.0\,m\,s^{-1}$ from 64° with a 2–22 m temperature difference of 0.72 °C. During the episode at the end of December, the average wind was lighter at $2.5\,m\,s^{-1}$ from 78° with a 2–22 m temperature difference of 0.77 °C. A fourth period of interest in Figs. 7(a) and (b) is just prior to Day 335 when the BL depth appears to increase significantly and the wind speed is higher while, surprisingly, [NO] remains extremely high as seen in Table 1.

In particular, Table 1 compares both meteorology and [NO] for shorter periods of maximum [NO], namely Days 327–330, Days 332–335, Day 335, and Days 355–358. More interesting, however, with similar mixing-layer depths and higher wind speeds, the first period shows much higher levels of [NO] than the last period. The second period, and Day 335 in particular shows high [NO] despite a much deeper mixing layer depth and much higher wind speed. In fact on Day 335 there is no shallow stable layer. The only obvious differences between the first two periods and the last one lie in the fact that in the first periods, in late November, there had been a sustained statically stable downslope flow off the high plateau for at least 10 days whereas the last event, in late December, followed an extended period of well-mixed, windy, cloudy, and sometimes convective conditions. Another consideration is the

Please cite this article as: Neff, W., et al., A study of boundary layer behavior associated with high NO concentrations at the South Pole using a minisodar, tethered balloon, and..., Atmospheric Environment (2007), doi:10.1016/j.atmosenv.2007.01.033

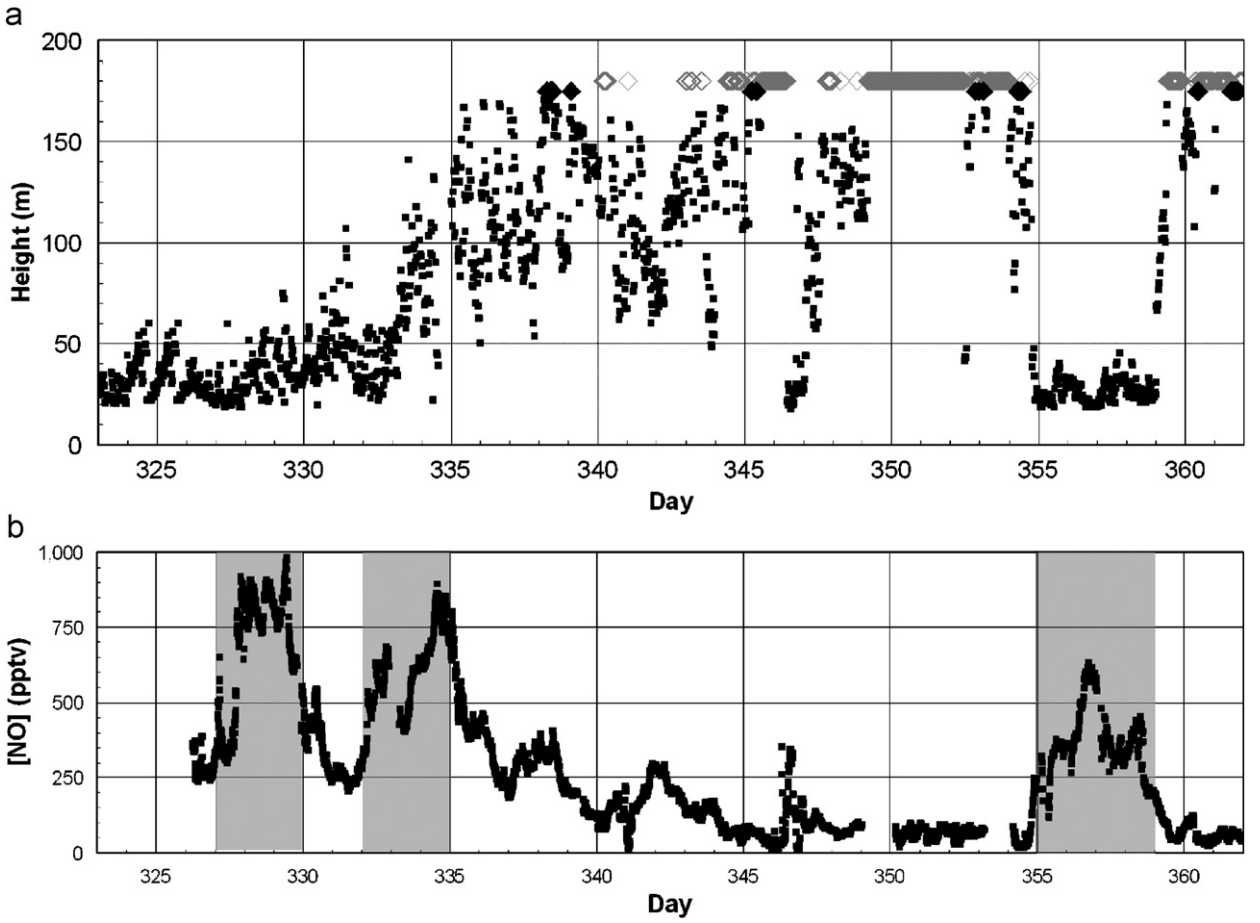

Fig. 7. (a) Time series of sodar-derived 0.5-h averaged mixing-layer height (solid squares) for Days 323–362 of the ANTCI experimental period. Elevated capping inversions are indicated by solid diamonds (175 m); periods of no detectable mixing layer top within the range of the sodar are indicated by open diamonds (180 m). (b) Time series of [NO] for the same period with multi-day periods from the Table 1 indicated by shading.

Table 1
Comparison of meteorology and [NO] for shorter periods of maximum [NO]

Period	Wind speed ($m\,s^{-1}$)	Wind direction (deg)	ΔT for 22–2 m (°C)	Sodar mixing layer depth (m)	[NO] (pptv)
Days 327–330	3.7	75	0.71	33.7	684
Days 332–335*	4.7	90	Missing	64.7	560
Day 335	5.2	95	0.07	108.0	483
Days 355–358	2.4	82	0.78	26.9	435

*Averaging carried out only where all variables were available except: ARO tower data missing for Days 333.3–335.04, wind speed and direction obtained from the automatic weather station at the South Pole and adjusted to 17 m. The adjustment was a factor of 1.29 based on the ratio of measurements at 2 and 17 m obtained on Day 332; Sodar data missing for Days 334.54–335.0.

potential variability in snow nitrate as suggested in the modeling analysis of (Wang et al., 2007). Another factor may result from longer accumulation times over the high plateau (Davis et al., 2004). However, the absence of either meteorological or chemical measurements on higher elevations to the east of the South Pole does not allow us to evaluate these two hypotheses.

Please cite this article as: Neff, W., et al., A study of boundary layer behavior associated with high NO concentrations at the South Pole using a minisodar, tethered balloon, and..., Atmospheric Environment (2007), doi:10.1016/j.atmosenv.2007.01.033

4.2. Dependence of [NO] on mixing height and surface turbulence

Fig. 8 shows a comparison of the height–[NO] relationship for early and late periods during the ANTCI experiment. The figure also includes the best-fit line from Davis et al. (2004) which used heights estimated using a spectral-peak estimation method developed by Oncley et al. (2004). (In this spectral method, the range of heights inferred from the analysis is much smaller than the range observed with the sodar: this may reflect differences in the experimental periods or the possibility that spectra near the surface do not reflect processes through the entire stable BL). The results in Fig. 8 show that there appears to be no simple relationship between [NO] and mixing-layer depth which is consistent with the suggestions of (Davis et al., 2004) that a number of processes can affect [NO] and the possibility that snow nitrate has significant temporal and spatial variability over the high Plateau. These results also speak to the value of the sodar data in providing a consistent measurement of mixing-layer depth in the evaluation of the various factors that influence [NO] at the South Pole and in the assessment of numerical simulation experiments (Wang et al., 2007).

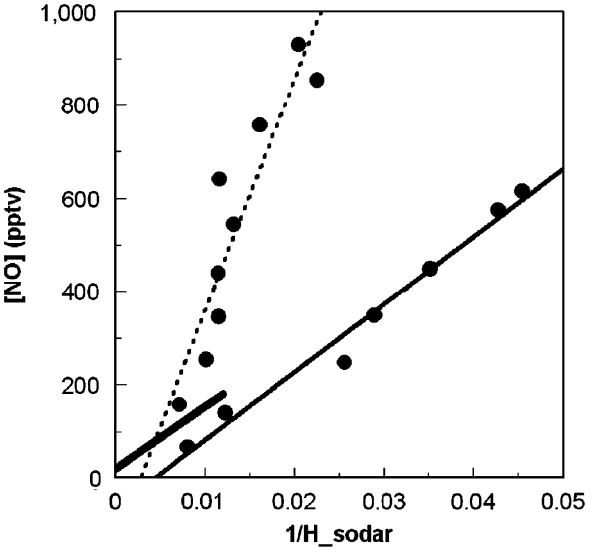

Fig. 8. Comparing binned [NO] and sodar mixing height data for early (Days 326–335: dashed line) and late (Days 355–359: solid line) experimental periods. Results reported by (Davis et al., 2004) are shown by the short solid line. Note that these latter data, based on indirect estimates, have a more limited height range than those observed with the sodar.

One can examine the dependence of [NO] on surface stress at 2 m, u_* (given by the covariance $\overline{u'w'_{2m}}$). The surface stress can be seen as one measure of the strength of turbulence that will diffuse NO upward into the BL. Fig. 9 shows the relation between [NO] and u_* for the period 12–29 December 2003, using binned [NO] data. With a correlation of $r^2 = 0.97$, it is clear that [NO] depends inversely on u_* for this period. The results in Figs. 8 and 9 also suggested a strong inter-relationship between NO, the boundary layer depth, and u_* as a measure of the strength of the mixing processes at the lower boundary.

The 2003 ANTCI data are still intriguing, however, in regards to the interpretation one might give concerning the effect of mixing-layer depth on [NO]. In particular, Davis et al. (2004) have shown that the lifetime of NO_x is a function of its concentration (their Fig. 8). Given a fixed NO_x flux of 3.9×10^8 molecules $cm^{-2}\,s^{-1}$ (Oncley et al., 2004) and the assumption of a mixing layer of ~20 m in depth, Davis et al. (2004) found that [NO] in excess of 400 pptv could be generated (their Fig. 10(a)). However, Fig. 7 shows [NO] exceeding 500 pptv for mixing-layer depths in excess of 100 m. Specifically, as shown in Fig. 7, over a short time interval on Day 334, [NO] approached 900 pptv and the mixing layer is greater than 100 m in depth. Although the 22-m tower data were not available at this time, the 0828-UTC rawinsonde and sodar data confirm the deep

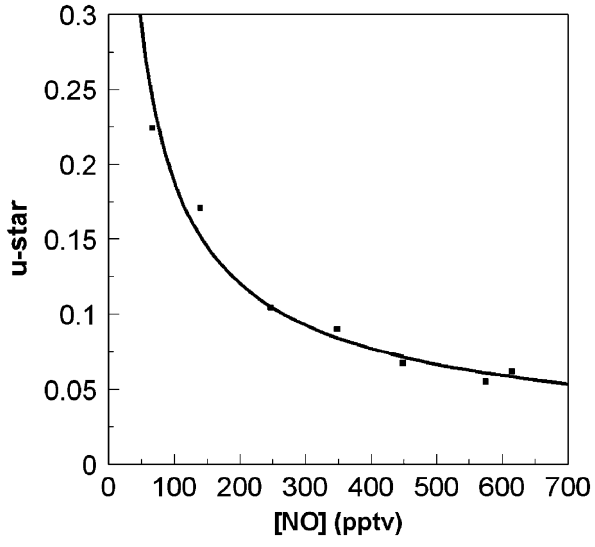

Fig. 9. Surface stress u_* (*u*_star) averaged for [NO] binned in 100 pptv intervals for Days 346–362.

Please cite this article as: Neff, W., et al., A study of boundary layer behavior associated with high NO concentrations at the South Pole using a minisodar, tethered balloon, and..., Atmospheric Environment (2007), doi:10.1016/j.atmosenv.2007.01.033

mixing layer that was present (Fig. 10). The rawinsonde reveals an almost adiabatic temperature profile to 100 m with relatively strong downslope winds while the sodar data confirm stable lamina above 125 m, which overlie a well-mixed layer (indicated by the descending striations indicative of large eddies in the BL.) There appear to be several factors involved in explaining this unique time period.

First, as outlined by Davis et al. (2004), the NO_x flux used in the earlier model studies may have a sizable uncertainty. Flux evaluations are quite challenging experimentally and their accuracy for a one-time effort, as carried out at SP using the modified Bowen Ratio technique, may be no better than a factor of two and perhaps worse. If one were to double the flux, the BL depth could be doubled and still achieve the same NO_x concentration level. Further information is available from Wang et al. (2007), who have inferred the NO emission fluxes required to produce the observed concentrations of NO_x (using a 1-D model with some model adjustments to better approximate observed sodar mixing layer depths). Their results are consistent with at least a factor-of-three variation in flux through the observing period, with peaks in the early period, 28 November–3 December, of about 6×10^8 molecules $cm^{-2} s^{-1}$. However, during this early period, the model underestimates the BL depth by a factor of two suggesting the NO_x flux could be perhaps a factor-of-two larger.

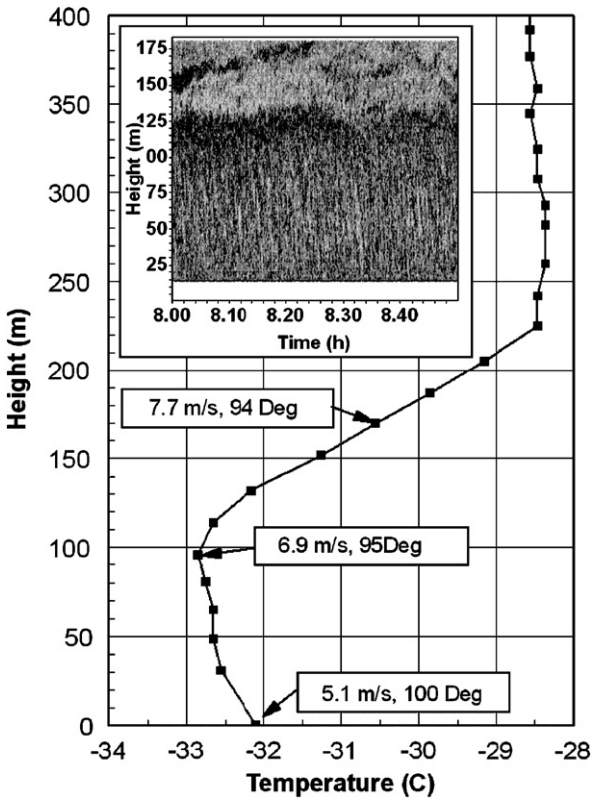

Fig. 10. Radiosonde sounding (launched at 0828 UTC) and sodar data (0800–0850 UTC) for Day 334 when [NO] was increasing from about 600 pptv to almost 900 pptv. The wind speed and direction are indicated at several heights.

A second issue involves a lack of knowledge of the morphology of BL flows that originate to the east of South Pole Station. For example, one might speculate that thin BLs might have formed on the higher plateau to the east and that these air parcels eventually would flow toward lower elevations like the South Pole. During this transport period, however, there could be a deepening of the BL (such as below the 4.5 °C capping inversion shown in Fig. 10). Thus, during an initial period involving a thin-layer phase on the high plateau, the nonlinear chemistry described earlier could have generated exceptionally high [NO]. As the air parcels passed over the high plateau toward the South Pole and the mixing layer steadily increased in depth, further accumulations of NO could have compensated for the vertical expansion. In this way, the final parcel sampled at Pole could have both the characteristics of moderate BL and very high [NO]. It is also interesting to note that during the period shown in Fig. 10, Arimoto et al. (2007) found high levels of sodium (from sea salt) and methanesulfonate (MSA, which has a marine origin), which the majority of their trajectory analyses indicated may have originated from the Indian Ocean side of the continent near 120°E.

Yet a third factor may also lie in the pattern of snow accumulation and loss at the SP. Significant accumulation of snow occurred in September (~0.11 m, during a period of record high winds which may have resulted in extensive drifting: ⟨ftp://amrc.ssec.wisc.edu/pub/southpole/⟩ followed by ablation and/or erosion of the snow in October (−0.05 m) and November (−0.01 m). One must then question whether high-nitrate snow was exposed in the ablation/erosion process leading to the high NO flux values inferred in the modeling results of Wang et al. (2007). These results suggest that much more needs to be learned about the distribution and recycling of snow nitrate over the high plateau. For these reasons, future studies would do well to

Please cite this article as: Neff, W., et al., A study of boundary layer behavior associated with high NO concentrations at the South Pole using a minisodar, tethered balloon, and..., Atmospheric Environment (2007), doi:10.1016/j.atmosenv.2007.01.033

provide more extensive surface and profile chemical and meteorological data over the high plateau as well as better characterization of snow nitrate concentrations.

4.3. Depth scaling from surface turbulence data

The availability of both profile information and surface turbulence data suggested a closer look at potential scaling laws that might apply to the stable BL at the South Pole. One motivation for such an analysis is the possibility of using a more limited instrument suite to infer mixing-layer depth in future field programs. The development of simple scaling laws for the stable BL has received considerable attention in the literature (e.g. Vickers and Mahrt, 2004; Zilitinkevich and Baklanov, 2002; Zilitinkevich et al., 2002) with a broad range of diagnostic equations having been proposed. Application to the conditions at the South Pole provides a unique opportunity because the location's lack of a diurnal cycle of insolation makes it possible for the BL to approach equilibrium depths: At sites further away from the South Pole, the presence of a diurnal cycle can lead to periods of thermal convection and highly effective vertical mixing, particularly over the high part of the Antarctic Plateau where latent heat effects are small (Argentini et al., 2005; King et al., 2006). Such convection limits the ability of the BL to achieve an equilibrium state.

Early studies at the South Pole (Neff, 1980), using a high-resolution 1-D numerical model, examined several scaling approaches. Observationally, those using parameters derived from the surface heat flux were problematic because of the small and highly variable flux values (due to rapid variations in the surface radiation balance). In this early work, model results documented the very slow response of the BL depth to changes in the surface cooling rate (~10 h) leading to inconsistencies in short-term observational comparisons. However, a measure of success was obtained using the very simple expression of Pollard et al. (1973):

$$H = 1.2u_*(fN_B)^{-1/2}, \tag{4}$$

where f is the Coriolis parameter, and N_B is the Brunt–Väisälä parameter given by

$$N_B = \frac{g}{T}\sqrt{\frac{\partial\theta}{\partial z}}. \tag{5}$$

Note that this formulation for H is relatively insensitive to the vertical potential temperature difference insofar as it occurs as a fourth root. The Pollard et al. relationship was derived as an equilibrium solution after invoking a constant stress at the surface of a rotating fluid with an initial, constant N_B where erosion of turbulence into the fluid is arrested after one inertial period (at the South Pole this is 12 h). A zero heat flux is assumed, which is not unreasonable for the South Pole data with heat losses of less than $5\,W\,m^{-2}$ under clear sky, stable conditions. Both this formulation and the following alternative based on eddy viscosity scaling have been described by Zilitinkevich et al. (2002):

$$H = C_S^2(u_*L/|f|)^{1/2}, \tag{6}$$

where $C_S \sim 0.7$ and L is the Obukhov length given by

$$L = -u_*^3T_o/kgQ_o, \tag{7}$$

where T_o is the temperature, Q_o the surface heat flux, k the von Karman's constant (~0.4). An early version of this expression was given by Zilitinkevich (1975) and examined using a numerical model by Brost and Wyngaard (1978) with reasonable success. Zilitinkevich et al. (2002), however, argue that while Eq. (6) works well at mid-latitudes, the fact that it overestimates the depth at high latitudes (King and Turner, 1997), may be due to nonlocal effects associated with vertical wave propagation. The unique data set from the South Pole motivated an examination of both expressions.

Fig. 11(a) shows the results of applying Eq. (4) for cases with downward heat fluxes and positive vertical temperature gradients. The temperature difference was calculated using both the 2- to 22-m difference as well as that measured by the rawinsonde (and then used for the subsequent 12-h period). In general, for shallow mixing layers, Eq. (4) gives reasonable results, but overestimates the depth as the mixing layer becomes deeper. The use of the twice daily rawinsonde data gives estimates that have more scatter but are not inconsistent with the results using the higher resolution 22-m tower data, reflecting the weak dependence in Eq. (4) on the vertical temperature difference.

Because both Eqs. (4) and (6) reflect equilibrium solutions (over at least the inertial period of 12 h), interpretation of the sodar data is a bit more complicated. Namely, because of changes in wind speed and stability during a day, a residual layer effect may arise as periods of increased mixing may cause the BL to grow followed by a collapse as

Please cite this article as: Neff, W., et al., A study of boundary layer behavior associated with high NO concentrations at the South Pole using a minisodar, tethered balloon, and..., Atmospheric Environment (2007), doi:10.1016/j.atmosenv.2007.01.033

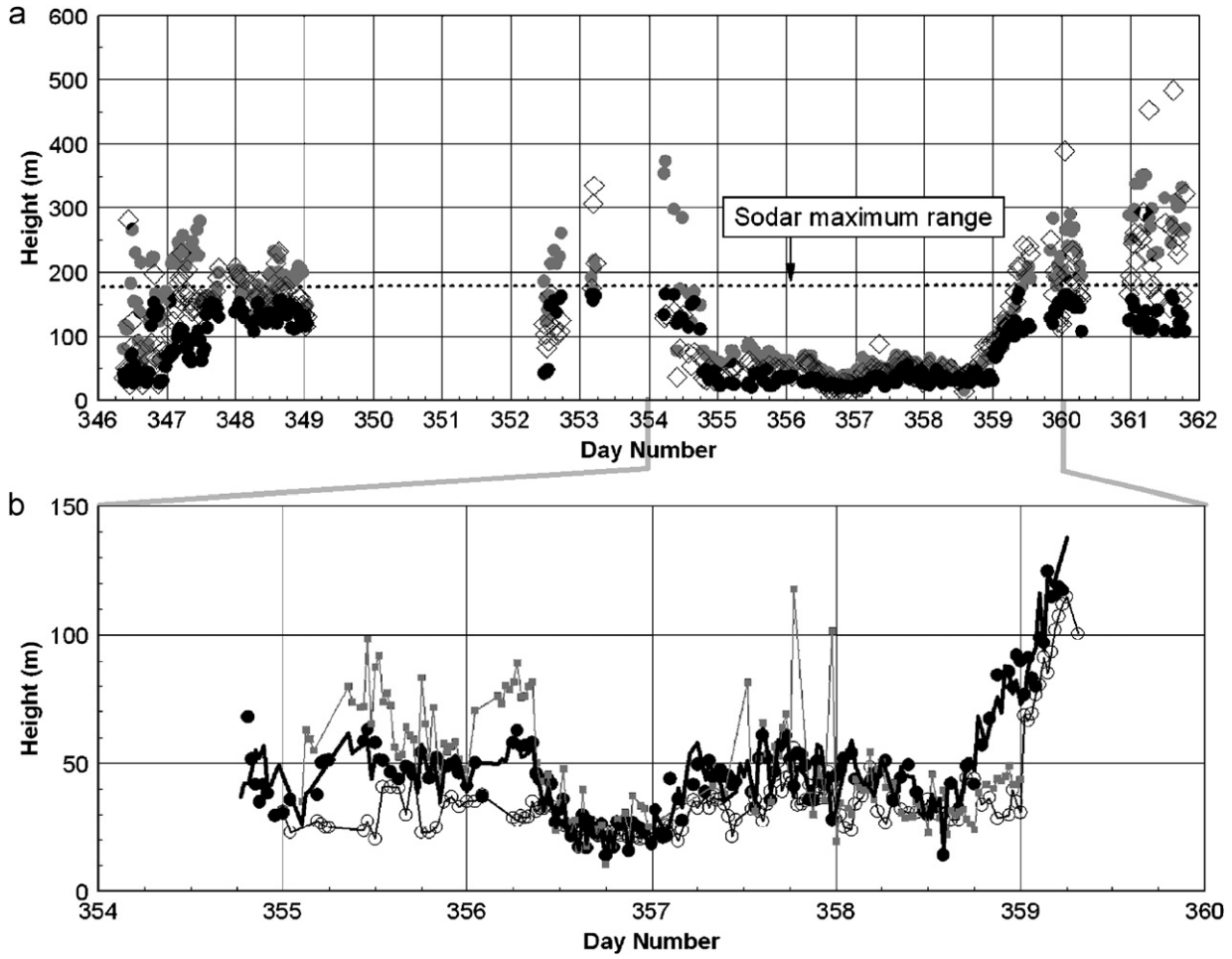

Fig. 11. (a) Time series of sodar-observed mixing depth (solid circles) with estimates using Eq. (4) based on vertical temperature gradients from the 22-m tower (gray circles) and the twice-daily rawinsonde (open diamonds, calculated for the 12 h following each sounding) and (b) time series for Days 355–359 for sodar-derived mixing depth (open circles, thin line) and that estimated from Eq. (4) (thick line), from Eq. (6) (gray line/solid squares), and with echo half-amplitude height (solid circles).

surface stability increases at times. The result in the sodar record is then a multi-layered structure whose 0.5-h averaged profile appears like that in Fig. 6(b), where no clear peak amplitude is present. Thus, for the persistent shallow layer period for Days 355–359, we also estimated the depth from the sodar data using the half-amplitude height in the profile with the results shown in Fig. 11(b) where we also compare the predictions from both Eqs. (4) and (6). As can be seen in the figure, the peak-detection method emphasizes shorter term internal boundary layers, which may actually be most relevant to surface mixing processes, whereas the half-amplitude method produces results more consistent with Eq. (4). Thus, we will assert that the sodar, under stable conditions provides both a quasi-equilibrium depth that reflects the history of the flow as well as the instantaneous depth that is more likely to represent current mixing conditions and is more relevant to surface [NO].

4.4. Implications for vertical diffusion

It should also be noted that Fig. 3 showed that the highest [NO] occurred at the bottom of what we have identified as the "mixing layer," which we characterized as an upper boundary for the mixing. Because stable BLs are characterized by very slow upward diffusion (Brost and Wyngaard, 1978), short-term variability in surface processes may

Please cite this article as: Neff, W., et al., A study of boundary layer behavior associated with high NO concentrations at the South Pole using a minisodar, tethered balloon, and..., Atmospheric Environment (2007), doi:10.1016/j.atmosenv.2007.01.033

dominate the surface accumulation of NO compared to the depth reflected in the sodar echo layer analysis. Therefore, it seemed useful to estimate the vertical diffusion times using the data available from ANTCI 2003. For example, Brost and Wyngaard (1978) pointed out the slow diffusion of changes at the surface into a stable BL using a crude scaling approximation based on the turbulent analogy to molecular diffusion: the diffusion time

$$\tau = H^2/K_M, \tag{8}$$

where H is the depth of the BL and K_M the exchange coefficient for momentum where the streamwise covariance for the turbulent vertical momentum transfer is given by

$$\overline{u'w'} = -K_M \partial U/\partial z. \tag{9}$$

Brost and Wyngaard point out that K_M peaks at a height of between $0.1H$ and $0.2H$ with $K_M(\max) = 0.03ku_*H$. This approach provides the maximum value of K_M. Thus,

$$\tau \sim H^2/(0.03ku_*H) = H/0.03ku_*, \tag{10}$$

provides a minimum estimate of the vertical diffusion time scale. For example, with $H = 20$ m, $k = 0.35$, and $u_* = 0.1\,\mathrm{m\,s^{-1}}$, then $\tau \sim 5$ h. Because we did not have measurements of the vertical shear of the horizontal wind. We used the expression $\overline{w'\theta'} = -K_H \Delta\theta/\Delta z$ to estimate K_H and assumed that $K_H \sim K_M$, i.e. a turbulent Prandtl number of order unity (as a very rough estimate in the absence of wave phenomena). We used a $\Delta\theta$ measured between 2 and 22 m (essentially between $0.06H$ and $0.7H$ for $H = 30$ m). The temperature flux was measured at 2 m. This calculation for Days 355–359 produced a mean diffusion time of 8.9 ± 2.9 h. The implication for [NO], following the calculations of (Davis et al., 2004), is that for the purposes of estimating when nonlinear chemistry might kick in, the "effective" mixing depth for NO could be much lesser than that observed by the sodar. For example, long vertical-diffusion times would favor nonlinear NO chemistry in the lowest portion of the boundary layer. The latter argument is not inconsistent with the [NO] profile shown in Fig. 3(a). However, the major uncertainty in this argument lies in not being able to quantify the NO loss terms as a function of height in these very stable conditions.

5. Conclusions

The 2003 ANTCI experiment provided an extensive followup to the 2000 and 1998 ISCAT experiments, seeking to understand the origin of extremely high surface concentrations of NO at the South Pole. Here, we have focused on the interpretation and analysis of acoustic sounder, or sodar, measurements of the BL. The sodar provided extensive insights into the BL behavior between 15 and 180 m over the entire ANTCI experimental period. Our height-detection routine provided estimated mixing-layer heights from the sodar at 0.5 h intervals, corresponding to the averaging time used in the processing of surface turbulence fluxes. Analysis of these heights confirmed a strong inverse relation to surface [NO] as found in early work. While the sodar deployment in ANTCI was designed specifically to detect shallow boundary layers, future field programs would be well advised to use high and low modes so as to capture the full inversion depth as well as its shallow boundary layer component.

Analysis of surface turbulence data using simple diagnostic expressions showed success with very shallow (<50 m) mixing layers and overestimation for greater depths in comparison with sodar data. The surface stress was found to be the most robust surface parameter controlling boundary layer mixing. Comparison with balloon profiling of [NO] suggested that the sodar-determined mixing height was only an upper bound on the "effective" mixing height with slow diffusion a likely explanation for the rapid falloff with height of [NO] within the mixing layer. One of the dominant features on the high plateau that led to shallow mixing layers and high [NO] was the presence of low-level jets with wind maxima at heights typically between 20 and 40 m. Because of the zero wind shear at the wind maximum and resulting large Richardson number, turbulence as well as chemical exchange with the surface was confined below this level.

Concerning the relationship between BL depth and [NO], we found two subseasonal regimes. Observations in the last half of December were consistent with the hypothesis developed from the earlier experiments, namely that very shallow BLs (occurring under light wind, strong stability conditions), on the order of 20 m deep, in conjunction with nonlinear NO_x chemistry can lead to high concentrations of NO. Conditions during late December ranged from windy, convective BLs (with low-to-moderate [NO], <100 pptv) to very shallow

Please cite this article as: Neff, W., et al., A study of boundary layer behavior associated with high NO concentrations at the South Pole using a minisodar, tethered balloon, and..., Atmospheric Environment (2007), doi:10.1016/j.atmosenv.2007.01.033

ones (with high [NO], 100–600 pptv). During this period, prolonged accumulation times on the high plateau prior to the South Pole episodes were unlikely. However, during late November and early December, [NO] was sustained at persistently high levels despite a mixing layer that reached over 100 m in depth at times in concert with higher winds and weaker stability. This regime, unlike that during the late December period, was preceded by conditions (lighter winds, strong stability) that could have been conducive to high [NO] and further accumulations of NO could have compensated for increasing BL depths during air parcels' movement toward South Pole. In addition, modeling results of Wang et al. (2007) suggest that much larger fluxes of NO from the snow characterized this earlier period. Thus, from an observational perspective we also found that the sodar provided a consistent measurement method with which to compare two distinct [NO] regimes and conclude that future programs look more carefully at the spatial and temporal variability of snow nitrate levels and the low-level parcel trajectories over the high plateau. In addition much still needs to be learned about the recycling of NO and its relation to snow accumulation/ablation/erosion processes over the Antartic high plateau.

Acknowledgments

D. Gottas and S. Abbott supported the development and deployment of the sodar system. We are grateful to S. Oncley of the National Center for Atmospheric Research for the loan of the sonic anemometer and helpful discussions in planning the analysis for the 2003 ANTCI experiment. We also appreciate the valuable comments of two anonymous reviewers. Funding for the ANTCI field program was received from the National Science Foundation, Office of Polar Programs, Grant #0230046. E. Dutton provided radiation data while T. Mefford made the GMD tower temperature data available. Any opinions, findings, and conclusions or recommendations expressed in this material are those of the authors and do not necessarily reflect the views of the National Science Foundation or the National Oceanic and Atmospheric Administration.

References

Argentini, S., Viola, A., Sempreviva, A., Petenko, I., 2005. Summer boundary-layer height at the plateau site of Dome C, Antarctica. Boundary-Layer Meteorology 115, 409–422.

Arimoto, R., Zeng, T., Wang, Y., Khaing, H., Huey, G., Davis, D., 2007. Concentrations and sources of aerosol ions and trace elements during ANTCI-2003. Atmospheric Environment, this issue.

Brost, R.A., Wyngaard, J.C., 1978. Model study of stably stratified planetary boundary-layer. Journal of the Atmospheric Sciences 35, 1427–1440.

Carroll, J.J., 1982. Long-term means and short-term variability of the surface-energy balance components at the South-Pole. Journal of Geophysical Research 87, 4277–4286.

Cohen, L., Helmig, D., Neff, W., Grachev, A., Fairall, C., 2007. Boundary-layer dynamics and its influence on atmospheric chemistry at summit, Greenland. Atmospheric Environment, in press, doi:10.1016/j.atmosenv.2006.06.068.

Davis, D., Nowak, J., Chen, G., Buhr, M., Arimoto, R., Hogan, A., Eisele, F., Mauldin, L., Tanner, D., Shetter, R., Lefer, B., McMurry, P., 2001. Unexpected high levels of NO observed at South Pole. Geophysical Research Letters 28, 3625–3628.

Davis, D., Chen, G., Buhr, M., Crawford, J., Lenschow, D., Lefer, B., Shetter, R., Eisele, F., Mauldin, L., Hogan, A., 2004. South Pole NO_x chemistry: an assessment of factors controlling variability and absolute levels. Atmospheric Environment 38, 5375–5388.

Eisele, F., Davis, D., Helmig, D., Oltmans, S., Neff, W., Huey G., Chen, G., Crawford, J., Arimoto, R., Buhr, M., Mauldin, L., Hutterli, M., Dibb, J., Blake, D., Roberts, J., Wang, Y., Tan, D., Flocke, F., 2007. ANTCI 2003 overview paper. Atmospheric Environment, this issue.

Helmig, D., Johnson, B., Oltmans, S., Neff, W., Eisele, F., Davis, D., 2007a. Elevated ozone in the boundary layer at the South Pole. Atmospheric Environment, this issue, doi:10.1016/j.atmosenv.2006.12.032.

Helmig, D. Johnson, B., Warshawsky, M., Morse, T., Neff, W., Eisele, F., Davis, D., 2007b. Nitric oxide in the boundary layer at the South Pole during the Antarctic Tropospheric Chemistry Investigation (ANTCI). Atmospheric Environment, this issue.

King, J.C., Turner, J., 1997. Antarctic Meteorology and Climatology. Cambridge University Press, Cambridge, UK.

King, J.C., Argentini, S., Anderson, P., 2006. Contrasts between the summertime surface energy balance and boundary layer structure at Dome C and Halley stations, Antarctica. Journal of Geophysical Research 111.

Neff, W., 1980. An observational and numerical study of the atmospheric boundary layer overlying the east Antarctic ice sheet. Ph.D. Thesis, University of Colorado, Boulder, 272pp.

Neff, W., 1988. Observations of complex terrain flows using acoustic sounders: echo interpretation. Boundary-Layer Meteorology 42, 207–228.

Neff, W., Coulter, R., 1985. Acoustic remote sensing. In: Lenshow (Ed.), Probing the Atmospheric Boundary Layer. American Meteorological Society, Boston, pp. 201–236.

Oncley, S., Buhr, M., Lenschow, D., Davis, D., Semmer, S., 2004. Observations of summertime NO fluxes and boundary-layer height at the South Pole during ISCAT 2000 using scalar similarity. Atmospheric Environment 38, 5389–5398.

Pollard, R., Rhines, P., Thompson, R., 1973. The deepening of the wind-mixed layer. Geophysical Fluid Dynamics 3, 381–404.

Please cite this article as: Neff, W., et al., A study of boundary layer behavior associated with high NO concentrations at the South Pole using a minisodar, tethered balloon, and..., Atmospheric Environment (2007), doi:10.1016/j.atmosenv.2007.01.033

Vickers, D., Mahrt, L., 2004. Evaluating formulations of stable boundary layer height. Journal of Applied Meteorology 43, 1736–1749.

Wang, Y., Choi, Y., Zeng, T., Davis, D., Buhr, M., Huey, G., Neff. W., 2007. Assessing the photochemical impact of snow NO_x emissions over Antarctica during ANTCI 2003. Atmospheric Environment, this issue, doi:10.1016/j.atmosenv.2007.01.056.

Wyngaard, J., Izumi, J., Collins, S., 1971. Behavior of the refractive-index-structure function near the ground. Journal of the Optical Society of America 61, 1646–1650.

Zilitinkevich, S.S., 1975. Resistance laws and prediction equations for depth of planetary boundary-layer. Journal of the Atmospheric Sciences 32, 741–752.

Zilitinkevich, S., Baklanov, A., 2002. Calculation of the height of the stable boundary layer in practical applications. Boundary-Layer Meteorology 105, 389–409.

Zilitinkevich, S., Baklanov, A., Rost, J., Smedman, A., Lykosov, V., Calanca, P., 2002. Diagnostic and prognostic equations for the depth of the stably stratified Ekman boundary layer. Quarterly Journal of the Royal Meteorological Society 128, 25–46.

Please cite this article as: Neff, W., et al., A study of boundary layer behavior associated with high NO concentrations at the South Pole using a minisodar, tethered balloon, and..., Atmospheric Environment (2007), doi:10.1016/j.atmosenv.2007.01.033